# Micromachined Infrared Sensor Arrays on Flexible Polyimide Substrates

**Aamer Mahmood**
Dept. of Electrical Engineering,
University of Texas at Arlington
Arlington, TX, USA
aamer@uta.edu

**Shadi Dayeh**[1]
Dept. of Electrical Engineering,
University of Texas at Arlington
Arlington, TX, USA
sdayeh@ucsd.edu

**Donald P. Butler**
Dept. of Electrical Engineering,
University of Texas at Arlington
Arlington, TX, USA
dbutler@uta.edu

**Zeynep Çelik-Butler**
Dept. of Electrical Engineering,
University of Texas at Arlington
Arlington, TX, USA
zbutler@uta.edu

## Abstract

*This paper presents work on micromachined infrared detectors on flexible substrates. The detectors are made of semiconducting yttrium-barium-copper-oxide (YBCO) and are built on a 40-50 μm layer of polyimide (PI58578G) that serves as the flexible substrate. Two variants of micromachined infrared detectors have been fabricated. The first variant employs a mesa structure in which self-supporting Ti arms hold up the detector pixel. The second variant has a more planar topology with the detector being supported by a layer of silicon nitride. Surface micromachining is used to isolate the detectors from the substrate. After fabrication the polyimide is peeled off the carrier wafer and the devices are packaged and characterized. The 40x40 $\mu m^2$ microbolometers have responsivities ranging from $7.4x10^3$ V/W to $10^4$ V/W and detectivities ranging from $6.6x10^5$ cm-$Hz^{1/2}$/W to $10^8$ cm-$Hz^{1/2}$/W. These results are comparable to those obtained for devices made on a rigid silicon substrate. The effect of substrate heating is also investigated and found not to affect the detector performance.*

## INTRODUCTION

The future for microsensors on flexible substrates looks very promising in both the civil and military fields. Work presented in this paper contributes towards the strategic aim of developing temperature, pressure, tactile and flow sensors along with the associated readout circuitry and electronics embedded in a flexible substrate. Flexible substrates mean greater versatility as they can be made conformal to non-planar and non-rigid surfaces. In previous work, the development of non-micromachined detectors on flexible substrates has been published [1,2] as has been results on similar micromachined microbolometers on rigid silicon substrates [3,4,5,6]. This work presents micromachined microbolometers on flexible polyimide substrates. Two types of microbolometers have been fabricated. The first kind employs a mesa structure in which self-supporting Ti arms support the detector pixel made of semiconducting yttrium-barium-copper-oxide (Y-Ba-Cu-O referred to as YBCO) above the substrate plane. The second type of microbolometers employs a more planar geometry. The detector pixel lies on a layer of silicon nitride atop sacrificial polyimide. Trenches around the pixel in the nitride expose the polyimide, which is micromachined from underneath the detector by dry etching. Both microbolometers are isolated from the substrate to reduce thermal conductance from the detector to the substrate.

Bolometers are thermal detectors in which the incident infrared energy causes the temperature of the detector to change, which in turn changes the detector resistance. This change in resistance is characterized by the thermal coefficient of resistance (TCR);

$$TCR = \beta = \frac{1}{R}\frac{dR}{dT} \qquad (1)$$

Here $R$ is the dc resistance of the device and $dR/dT$ is the rate of change of the resistance versus temperature. A figure of merit for detector performance is the responsivity $R_v$, defined as the detector output voltage per input infrared power.

$$R_v = \frac{\eta \beta R I_b}{G_{th}\left(1+\omega^2\tau_{th}^2\right)^{1/2}} \qquad (2)$$

where $\eta$ is the optical absorption coefficient of the thermometer, $R$ is the dc resistance of the device, $\beta$ is the TCR, $I_b$ is the dc bias current, $G_{th}$ is the thermal conductance between the microbolometer and its surroundings, $\omega$ is the angular modulation frequency of the incident IR radiation and $\tau_{th}$ is the thermal response time of the detector. The thermal response time is defined as the ratio of the thermal capacitance to the thermal conductance of the microbolometer. Another important figure of merit is the detectivity $D^*$:

$$D^* = \frac{R_v\sqrt{A\Delta f}}{\Delta V_n} \qquad (3)$$

[1] Currently at University of California, San Diego.

where $\Delta f$ is the electrical bandwidth and $V_n$ is the total noise voltage observed in $\Delta f$. The detectivity is a form of area normalized signal-to-noise ratio.

This paper presents the detailed method of fabrication for two different types of micromachined microbolometers on flexible substrates. This is followed by a description of the characterization process. The experimental results are presented and discussed

## FABRICATION

Two different geometries were fabricated. The mesa geometry employed self-supporting Ti arms that supported the detector pixel (Figure. 1(a)). The trench geometry consisted of trenches around the pixels to expose the sacrificial polyimide beneath the silicon nitride layer supporting the detector pixel (Figure. 1(b)).

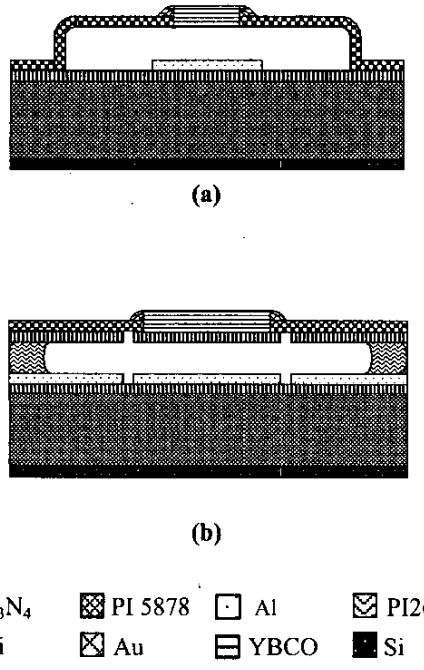


**Figure 1. Micromachined bolometers on flexible substrates (a) schematic of mesa geometry (b) schematic of trench geometry**

Despite the differences, the two geometries share the same initial fabrication steps. During fabrication, all depositions were done using an RF magnetron sputter system that was equipped with a turbo vacuum pump. The depositions were carried out in a pure Ar environment at 10-mTorr pressure using 3-inch targets. First, 4000A° of $Si_3N_4$ was sputtered on to the wafer using 200W of RF power. This layer of nitride helps in the adhesion and passivation of the subsequent polyimide to the wafer during the entire fabrication process. This was followed by spin coating liquid polyimide (PI5878G) onto the wafer. This process was repeated five times and the polyimide-coated wafer was then loaded into an oven at 110-115°C. The oven temperature was gradually ramped to 275°C and the polyimide was cured for 5 hours at 275°C. The final polyimide thickness after curing was 40μm. The polyimide was then coated with 4000°A of sputtered $Si_3N_4$. This layer serves as a passivation layer and also promotes adhesion between the polyimide and the subsequent layers sputtered during fabrication. The nitride is resistant to the wet etchants that will subsequently be used in this process. However, to protect it from dry etchants, a 500A° layer of $SrTiO_3$ was sputtered at 100W. Subsequent to this point, both detectors took different fabrication paths and are listed separately below.

### Mesa geometry

A 2600A° Al mirror was sputtered at 300W on the $SrTiO_3$ and patterned to form square reflector mirrors the same size as the final detector pixels. A photo definable sacrificial polyimide (PI2737) was spin coated onto the wafer and pre and post baked for 60 seconds at 65°C and 95°C respectively. The polyimide was exposed to UV light and developed. This resulted in a rectangular mesa structure over and around the pixel. Ti electrode arms were then patterned by lift-off using a 1.5μm thick negative photoresist. This was followed by sputtering 1000A° of Ti at 150W to form the contact arms between the YBCO detector and the bond pads. Ti was used as the contact arm material because of its low thermal conductivity 0.219W/cm-K.

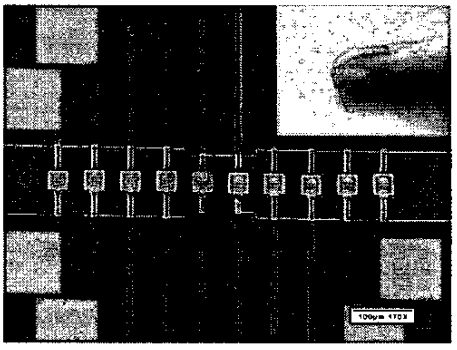

**Figure 2. SEM micrograph of 1x10 array of 40μmx40μm mesa geometry microbolometers and (inset) a section of the flexible substrate on a finger**

This minimizes heat loss from the detector to the substrate. This was followed by 700A° of Au sputtered at 100W over the Ti to form contact and bond pads. Au was patterned on the electrode arms using positive photolithography and wet etching with a $KI:I_2$ solution.

This defined the Au bond pads and the Au contacts to the subsequent YBCO detector pixel. A 4000A° layer of YBCO was then sputtered at 90W. The YBCO film was patterned using positive photolithography and etched with commercial Al etch solution. This created the detector pixel. The sacrificial polyimide (PI2737) layer was removed using $O_2$ plasma ashing at 120W RF power. The last step was to remove the polyimide substrate form the silicon wafer carrier yielding infrared sensors on a flexible substrate.

### Trench geometry

In the second geometry, the polyimide substrate was spin-cast and passivated using the same procedure as in the case of the mesa geometry. A 4000A° film of Al was deposited above the $SrTiO_3$ and served as a reflector under the detector for incident infrared energy. The Al was not patterned in the form of the YBCO thermistor rather it was patterned using the trench mask. Without compromising the electrical role of the reflector, this facilitated mask and wafer alignment at the terminal stages of the wafer fabrication. Sacrificial polyimide (PI2610) was spin coated above the Al, followed by a pre-bake. The polyimide-coated wafer was then loaded into an oven at 150°C. The oven temperature was gradually ramped to 275C and the polyimide was cured for 4 hours at 275°C. After curing, the final sacrificial polyimide thickness was 0.5μm. A 4000A° layer of $Si_3N_4$ was then sputtered onto the polyimide at 200W followed by 500A° of $SrTiO_3$.

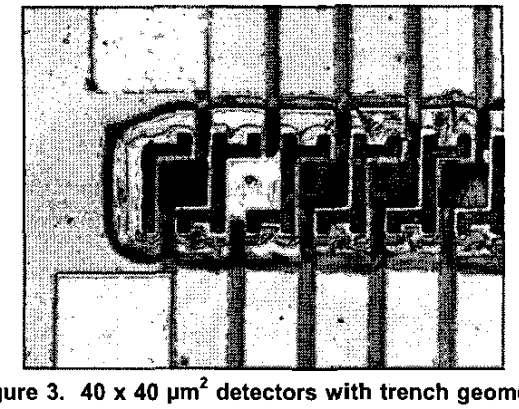

**Figure 3. 40 x 40 μm² detectors with trench geometry after 10 hours of ashing. The second pixel from the left has been removed and shows Al reflector surface sans polyimide**

The nitride serves as a passivation layer for the underlying polyimide and also promotes adhesion between the polyimide and subsequent layers. The $SrTiO_3$ serves as a protective layer for the nitride against dry etchants. 1500A° of Ti was then sputtered onto the wafer at 150W followed by 750A° of Au at 100W. The Au was patterned to form the contact pads between the subsequent Ti contact arms and the YBCO detector pixel as well as the bond pads. Ti was then patterned by dry etching in an environment of $CF_4$:$O_2$ in a ratio of 40:2 sccm. This yielded the contact arms between the aforementioned Au pads and contacts. The last deposition in the fabrication process was 3600A° YBCO sputtered onto the wafer. The YBCO was patterned and etched to yield the detector pixels (thermistors). Up to this point, the detector sat atop a solid mass. Trenches were opened around each pixel in the $SrTiO_3$. This exposed the underlying layer of $Si_3N_4$. The wafer was put in a reactive ion etcher and the exposed nitride was dry etched. Nitride was thus removed in the trench area exposing the underlying sacrificial polyimide PI2610. The sacrificial polyimide was removed by a gradual process of ashing. It has been observed that continuous ashing for long periods of time heats the wafer and produces thermal stresses in the layer of nitride supporting the detector. These stresses cause the nitride to become wavy and corrugated, thereby affecting the geometry and integrity of the YBCO pixel. To avoid this, the ashing was carried out in short 20 min bursts followed by a 10 min cooling period for the wafer. The cumulative ashing time was approximately 10 hours. At this stage, it was seen that the PI2610 beneath the smaller 40x40μm² pixels was removed completely (Figure 3.). While some polyimide remained beneath the larger 65x65μm² devices.

## CHARACTERIZATION

Electrical and optical characterization of the devices was carried out. The devices were packaged in ceramic packages and ultrasonically wire bonded. Bolometers were made in 65x65μm² and 40x40μm² sizes. It was seen that the smaller detectors performed better. Results presented here are generally for the smaller 40x40 μm² devices unless otherwise specified. Device "DD15" has a mesa geometry and device "1b4" has a trench geometry.

The dc resistance at 290K was 7.33 MΩ and 4.94 MΩ for "DD15" and "1b4" respectively. For the R-T (resistance-temperature) measurements, the devices were placed in a cryostat such that they were firmly in contact with a variable temperature platform. The cryostat was evacuated to about 100mT pressure. A Lakeshore 91C temperature controller controlled the temperature of the stage using a combination of a heater element and a Leybold RW3 closed cycle refrigerator. A resistance was connected in series with the device and one was connected in shunt with the device and the first resistance. An HP34401A multimeter used as an ohmmeter provided a fixed dc bias. The resistance of the detectors as a function of temperature was calculated

indirectly by measuring the voltages across both the resistors at different temperatures. The TCR was calculated using (1).

Resistance of device "DD15" was measured from 220 to 310 K (Figure 4(a)). It was found to have a TCR of -3.4 $\%K^{-1}$ at 290 K. Device "1b4" was measured from 240 to 320 K (Figure 4 (b)). It had a TCR of -2.9 $\%K^{-1}$ at 290 K. Thermal conductivity $G$, was measured using the Joule heating method. The detector and its ambient are kept at constant room temperature and any heating is solely due to Joule heating due to the current flowing through it. The heating causes the device resistance to change, which causes the device V-I characteristics to become non-linear. For device "DD15", an HP4142 DC source was used to vary a dc bias current from -2 to 2 μA. The thermal conductance $G$ was computed from the slope of the plotted resistance versus dissipated power using (4).

$$R(T) = R_0 + \frac{1}{G}\frac{dR}{dT} I_b^2 R(T) \qquad (4)$$

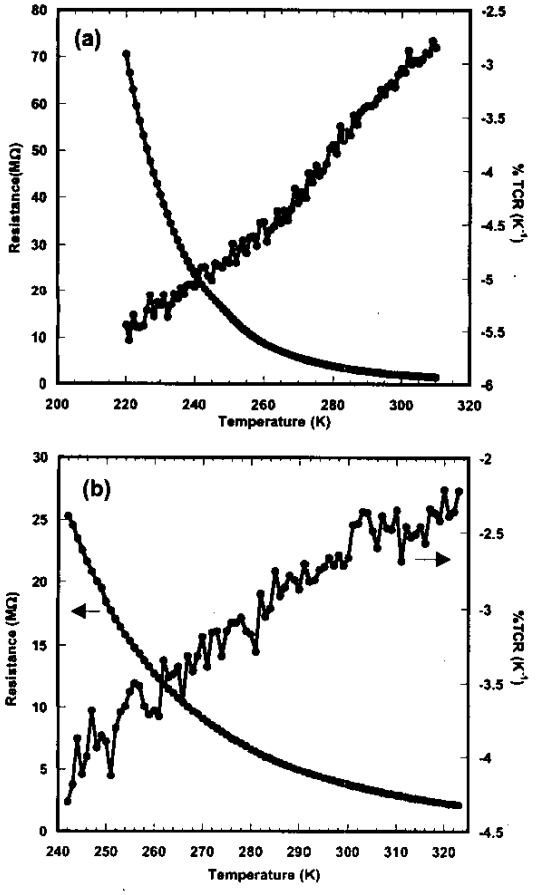


**Figure 4. Resistance and TCR versus temperature a) DD15, b) 1b4**

For device "1b4", the current sweep was done using the HP 4155B semiconductor parameter analyzer. The current was swept from -2 to 2 μA and $G$ was calculated from (4) from the slope of the device resistance versus power characteristic. Thermal conductivities of $4x10^{-7}$ W/K and $6.6x10^{-7}$ W/K were measured for "DD15" and "1b4" respectively. The thermal isolation of both these devices from the substrate is seen contributing to the very low G values.

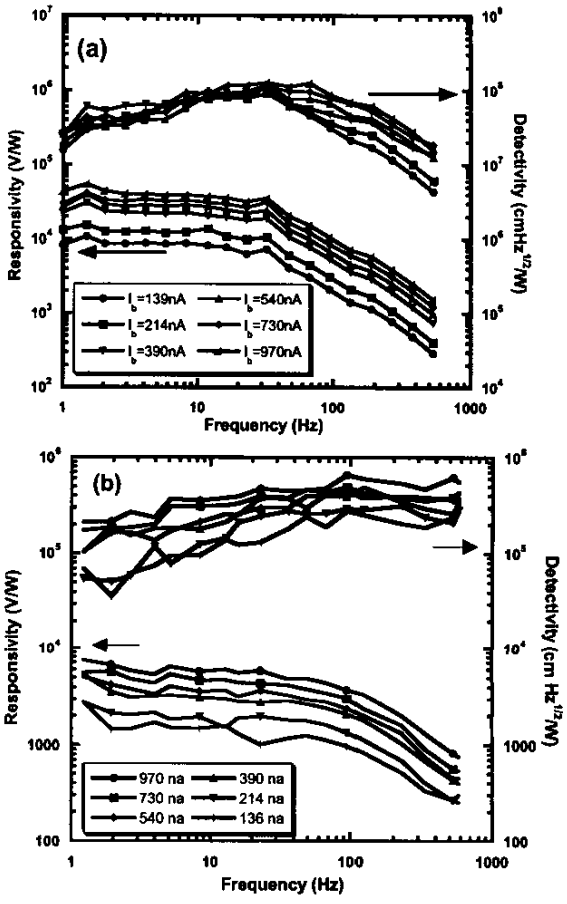


**Figure 5. Responsivity and detectivity measurements versus optical modulation frequency of a microbolometer a) DD15, b) 1b4**

The optical characterization was done using a blackbody IR source made by Infrared Industries. During the measurements, the source was kept at 990°C for "DD15" and 900°C for "1b4". The detector was biased by different dc currents ranging from 214 nA to 1 μA. The device output was measured by an HP 3562A signal analyzer through an EG&G PAR 113 low noise preamplifier to improve the signal to noise ratio. For calibration purposes, an Oriel 70124 pyroelectric detector with a responsivity of 1000V/W was used. The device

was mounted inside a cryostat and measurements were made in air as well as in vacuum with the cryostat evacuated to ~ 100 mTorr pressure. A chopper was used to modulate the infrared signal incident on the detector. Device "DD15" had a responsivity in the order of $10^3$V/W and $10^4$ V/W in air and vacuum respectively. Device "1b4" had a responsivity of $10^2$ V/W and $10^3$ V/W in air and vacuum respectively. The detectors perform better in vacuum as the air between the detector and the substrate serves as a path for heat conduction.

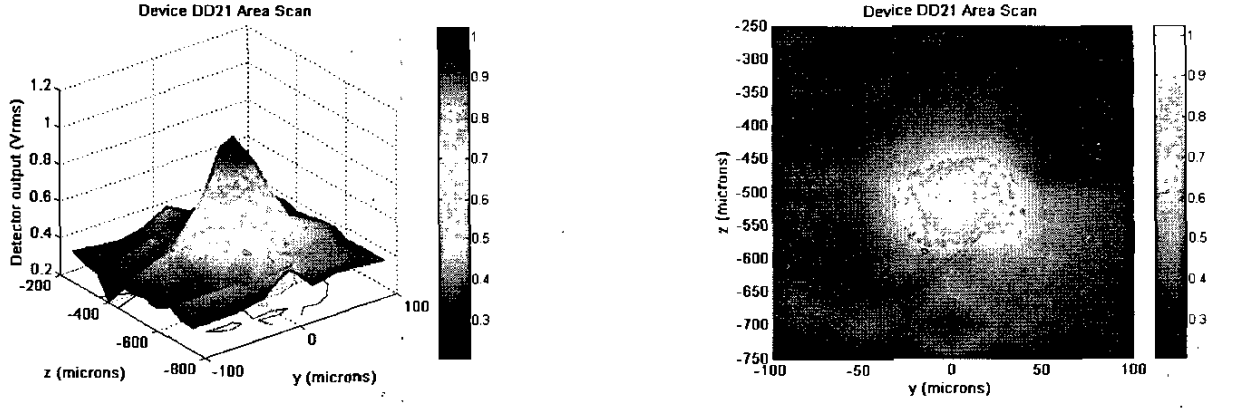


(a) (b)

**Figure 6. Device DD21 scanned by a point source of infrared light. Actual device dimensions are 65x65μm$^2$. (a) Isotropic view and (b) top view**

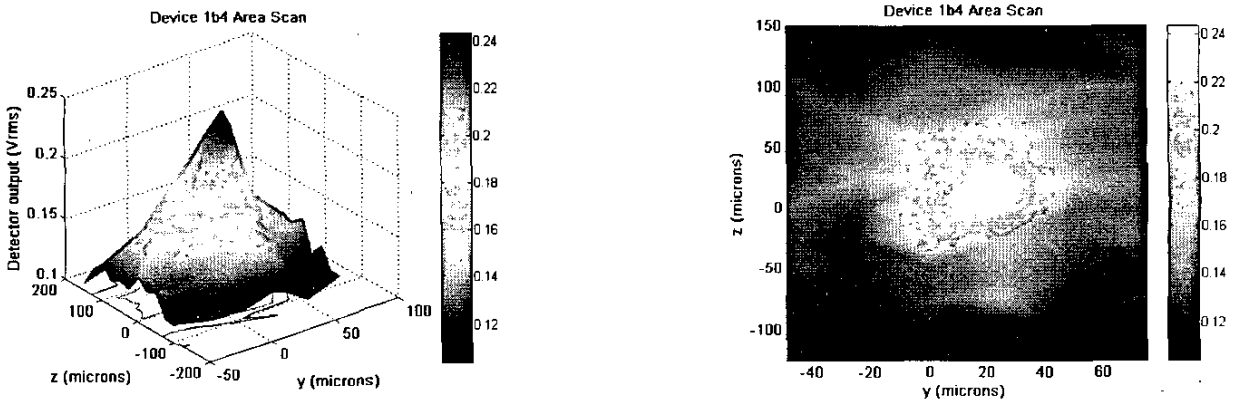


(a) (b)

**Figure 7. Device 1b4 scanned by a point source of infrared light. Actual device dimensions are 40x40μm$^2$. (a) Isotropic view and (b) top view**

Responsivities as high as $10^4$V/W and $7.4x10^3$ were measured for "DD15" and "1b4" respectively. In addition to the signal at the different chopper frequencies, the noise at these frequencies was also measured. Both the signal and the noise are used to calculate the device detectivity using (3). Detectivities of $10^8$ cmHz$^{1/2}$/W and $6.6x10^5$ cmHz$^{1/2}$/W for "DD15" and "1b4" have been measured. Figure 5 shows the responsivity and detectivity as a function of chopper frequency for both device "DD15" and device "1b4".

The effect of substrate heating on detector performance was also studied. The detectors were placed in a cryostat with a ZnSe window. A small aperture (400-500 μm in diameter) was placed in front of the blackbody source and

a ZnSe lens was used to focus the infrared energy onto the detector. The lens was fixed to an XYZ-axes translational stage controlled by a Newport MM3000 motion controller. In addition to focusing the spot of light, this also made moving the spot of infrared light on the detector plane possible. The device was biased by 1μA of current. An HP 3561A dynamic signal analyzer was used to record the detector output. A Stanford Research Systems Model SR 560 low noise amplifier was used to improve the signal to noise ratio before the signal analyzer. The area in the vicinity of the detector was scanned in steps of 25 μm and the detector output signal plotted using MATLAB. The resulting sharp images have dimensions comparable to those of the microbolometer pixels (65x65 $\mu m^2$ for "DD15" and "DD21" and 40x40 $\mu m^2$ for "1b4"). This shows that the devices only respond to infrared energy incident on the detector pixel. Substrate heating due to incident radiation has no effect on the detector performance.

## CONCLUSION

Two variants of surface micromachined microbolometers on flexible substrates have been presented. The detailed method of fabrication for both the mesa and the trench geometries has been described. The detectors have been characterized electrically and optically. Temperature coefficient of Resistance (TCR) ranging from -2.9 $\%K^{-1}$ to -3.4 $\%K^{-1}$ at 290K have been measured. Low thermal conductivities of $4x10^{-7}$ W/K and $6.6x10^{-7}$ W/K were measured. The responsivity of the detectors ranged from $7.4x10^3$ to $10^4$ V/W. The Detectivity ranged from $6.6x10^5$ cm $Hz^{1/2}$/W to $10^8$ cm $Hz^{1/2}$/W. The mesa geometry was found to be better than the trench geometry, with the device with mesa geometry "DD15" having an optical response an order of magnitude higher than the device with trench geometry "1b4". Both devices have thermal conductivities of the same order of magnitude which points towards the layer of $Si_3N_4$ supporting the detector in the trench geometry as the most probable cause of the lower optical response. The mesa geometry employed a detector supported by Ti arms without any $Si_3N_4$ bridge. Future work entails vacuum encapsulating the detectors with a polyimide superstrate as this will enable the devices to perform best without any external vacuum requirements. This will also contribute to greater mechanical strength as the device can be placed in a near-zero-stress plane between the top and bottom layers of polyimide.

## ACKNOWLEDGMENTS

The authors wish to acknowledge the help of Ronald Elsenbaumer, Jim Florence, Eduardo Maldonado, Guillaume Gbetibouo and Nasir Basit at the UT Arlington Nanofab center. This work is based in part upon the work supported by the NSF under grant ECS-0245612. The authors also thank the Cornell Nanofabrication Facility for fabricating the photolithography masks used in this work.

## REFERENCES

[1] Yaradanakul, A.; Butler, D. P. and Çelik-Butler, Z. , "Uncooled infrared microbolometers on a flexible substrate," IEEE Transactions on Electron Devices, **49**, 930 (2002).

[2] Yildiz, A.; Çelik-Butler, Z.; Butler, D. P., "Microbolometers in a flexible substrate for infrared detection," accepted for publication in IEEE Sensors Journal.

[3] Travers, C. M.; Jahanzeb, A.; Butler, D. P.; and Çelik-Butler, Z., "Fabrication of semiconducting YBaCuO surface-micromachined bolometer arrays, IEEE Journal of Microelectromechanical systems, **6**, 271 (1997).

[4] Jahanzeb, A.; Travers, C. M.; Çelik-Butler, Z.; Butler, D. P. and Tan, S. G., "A semiconductor YBaCuO microbolometer for room temperature IR imaging," IEEE Transactions on Electron Devices, **44**, 1795 (1997).

[5] Gray, J.E.; Çelik-Butler, Z. and Butler, D. P., "MgO sacrificial layer for micromachining uncooled Y-B-Cu-O IR microbolometers on $Si_3N_4$ bridges," IEEE Journal of Microelectromechanical Systems, **8**, 192, (1999).

[6] Almasri, M.; Butler, D. P. and Çelik-Butler, Z., "Self-supporting uncooled infrared microbolometers with low thermal mass," IEEE Journal of Microelectromechanical systems, **10**, 469 (2001).